Journal of the Energy Institute 105 (2022) 121–132

Contents lists available at ScienceDirect

Journal of the Energy Institute

journal homepage: www.elsevier.com/locate/joei

The influence of mineral addition on the Optimised Advanced Ash Fusion Test (OAAFT) and its thermochemical modelling and prediction

Patrick Daley [a], Markus Reinmöller [b,c], Orla Williams [a,*], Cheng Heng Pang [d], Edward Lester [a]

[a] Faculty of Engineering, University of Nottingham, University Park, NG7 2RD, Nottingham, United Kingdom
[b] Technical University of Denmark, DTU Engineering Technology, Lautrupvang 15, 2750, Ballerup, Denmark
[c] Technische Universität Bergakademie Freiberg, Institute of Energy Process Engineering and Chemical Engineering, Fuchsmühlenweg 9, 09599, Freiberg, Germany
[d] Department of Chemical and Environmental Engineering, The University of Nottingham Ningbo China, Ningbo, 315100, PR China

ARTICLE INFO

Keywords:
Advanced ash fusion test
Ash
Thermochemical modelling
FactSage
Minerals

ABSTRACT

Specific minerals in ash are triggers for ash fusion during combustion. This study analyses, for the first time, the link between individual minerals and the ash fusion of pseudo ash pellets using the Optimised Advanced Ash Fusion Test (OAAFT) and FactSage modelling. The study analysed 20 pseudo ash pellets whose composition spanned a wide range of fuels used in the power generation industry. Varying quantities of the 4 main minerals were used to create the pseudo pellets; CaO (0–40%), Fe_2O_3 (0–40%), MgO (0–25%), and Silica-Alumina ratio (0.5:1–4:1). The OAAFT produced characteristic ash fusion curves for the pseudo pellets and individual minerals. The study also gained insight into the link between mineral transformations and ash fusion by comparing these profiles to the slag formation predictions in the FactSage modelling. Excellent alignment was obtained between the OAAFT curves and FactSage data. The OAFFT curves can be described as individual fingerprints of the ash fusion behaviour of the sample, which can be broken down into individual components. This data cannot be obtained from the conventional ash fusion test. By combining OAAFT and FactSage data, power generators can replicate slagging and fouling issues and identify the major components which are causing issues. The addition of mineral additives can be tested to analyse how slagging and fouling issues can be tackled for specific fuels. This will be of increasing importance as fuel blending and new complex fuels such as refuse derived fuels enter the market.

1. Introduction

Ash deposition in boilers can occur as slagging and/or fouling [1]. Slagging and sintering (partial slagging of the deposits) occurs in the high-temperature radiant section of boilers, while fouling occurs on convective heat-transfer surfaces at relatively low temperatures [2]. Slagging and fouling are key issues for the power industry and cause significant problems with continuous, long-term boiler operation [3,4]. There are various methods to predict slagging and fouling, including dilatometry/shrinkage tests [5–7], sinter strength tests [8,9], viscosity measurements [10,11], a range of empirical indices [10,12–15], and the ash fusion test (AFT), which is one of the most popular methods [9,11,13,16,17]. The AFT was developed in the formative years of the power industry to predict clinker (large lumps of ash) forming characteristics in stoker furnaces [18]. It has recently been revised using modern image analysis techniques to plot the curve of the relative height of the ash pellet against temperature [19]. In addition to the traditional AFT parameters such as initial deformation temperature (IDT), the Optimised Advanced Ash Fusion Test (OAAFT) can quantify the extent of shrinkage and swelling during the test via the outputted characteristic curve for any given ash pellet based on image analysis [19,20]. Pang et al. [19] developed the advanced ash fusion test (AAFT). The AAFT uses automated image analysis to plot a curve of relative height of the pellet against temperature. The OAAFT took this work further to create a standardised test that is clearly repeatable whilst giving the best representation of the first point of melting [20]. The AAFT and OAFFT are the first innovations of the traditional AFT since its inception in the early 1900s [18].

Coal and biomass ash is generally made up of 4 major elements and accounts for over 90% of mineral matter in bituminous coal and wood pellets [21]. Other inclusions occur at lower average concentrations but can spike sporadically in some coals. These major minerals include

* Corresponding author.
E-mail address: orla.williams@nottingham.ac.uk (O. Williams).

https://doi.org/10.1016/j.joei.2022.08.004
Received 23 May 2022; Received in revised form 2 August 2022; Accepted 4 August 2022
Available online 17 August 2022

Al_2O_3, SiO_2, CaO, and Fe_2O_3 with lesser common minerals being MgO, K_2O, Na_2O, and SO_2. These oxides can be classes as acidic oxides (SiO_2, Al_2O_3 and TiO_2) and basic oxides (ex. Fe_2O_3, CaO, MgO, K_2O and Na_2O) based on their roles on the ash fusibility [22]. The ratio of these main mineral inclusions plays a pivotal role in determining melting characteristics [23]. The effect of individual minerals on ash fusion temperatures has been shown [11,24–27] but has not been investigated for the characteristic curve obtained from the OAAFT [19,20].

Empirical investigations of the main mineral components and their impact on ash fusion temperatures have been previously investigated [24–27]. The Silica-Alumina (S/A) ratio is an important parameter that affects the flow properties of coal ash slag [28]. Two key studies by Liu et al. [27] and Song et al. [26] have analysed the impact of varying mineral component ratios on the S/A ratio for 34 and 33 pseudo ashes, respectively. Both sets of ashes were composed of the four major elements Al_2O_3, SiO_2, CaO, and Fe_2O_3, however, Liu added K_2O, whilst Song added MgO. Each study found that higher Fe_2O_3 content resulted in lower AFT temperatures. The studies directly contradict each other with Liu finding that increasing the Silica-Alumina (S/A) ratio reduced ash fusion temperatures by 200 °C and Song finding the opposite [26,27]. The CaO content displayed a local minimum of AFT temperatures in both studies at 30% (Liu) and 35% (Song) weight but increase either side of this point. The latter minimum for Liu can be attributed to the reduced step size of added weight. The K_2O displayed no significant change in Lui's study, whilst Song found that increasing MgO generated an S-shaped curve, initially decreasing ash fusion temperatures, then increasing, before finally greatly reducing ash fusion temperatures. Niu et al. [24] carried out a study for synthetic biomass ashes, whilst not directly comparable to coal ashes due to the different composition, found an increase in base-to-acid (B/A) ratio reduces the IDT if the ratio is more than 0.7. A further study by Yan [28] focused only on the S/A ratio under inert conditions and found similar results to Liu, but also linked shrinkage to slag formation rate.

The five-component relationship of Al–Si–Ca–Fe–O has been used in the F*A*C*T computing package (predecessor of the FactSage software package) to predict the phase equilibria of coal ash slags [29]. Continuous improvement in predictive modelling of mineral transformation during heating of ash is being made using modelling software FactSage [30–35]. Furthermore, there have been successful attempts to validate Factsage models using pseudo ash samples [26,36,37]. However, the impact of individual components on the OAAFT curve, and its comparison to FactSage modelling has not been investigated.

The novel combination of the OAAFT and FactSage modelling offers an opportunity to better understand the link between triggers for ash melting and mineral transformations and in turn, can be used to enhance fuel selection and estimate additive blending predicting slagging and

Table 1
Pseudo pellet literature samples database - Major oxide compositions of a range of coals and their ash fusion temperatures [4,27].

	Ash Samples	Content of oxides				AFT temperatures (°C)			
		SiO_2	Al_2O_3	S/A	Fe_2O_3	CaO	MgO	IDT	FT
Chinese Coals	Shanxi Datong	56.6	25.4	2.2	6.5	3.7	1.4	1239	1352
	Heilongjiang Jixi	64.1	27.2	2.4	2.9	0.9	0.5	>1450	>1450
	Shandong Xinwen	52.9	31.9	1.7	4.9	2.7	1.2	>1450	>1450
	Anhui Huainan	50.8	36	1.4	6.1	1.9	0.6	>1450	>1450
	Neimenggu lijiata	41.7	23.0	1.8	7.1	13.1	2.1	1141	1177
	Liaoning Fuxin	52.7	33.5	1.6	5.9	1.8	1.1	>1450	>1450
	Shanxi Huating	39.7	18.2	2.2	17.1	17.5	0.9	1160	1300
	Shandong Zaozhuang	34.9	16.5	2.1	8.0	37.1	2.0	1180	1230
	Shandong yanzhou	23.0	34.0	0.7	22.1	17.3	1.7	1155	1225
	Shanxi gujiao	24.2	27.1	0.9	25.2	18	0.7	1220	1280
Imported Bituminous Coals	Sofia Bulgaria	32.0	11.3	2.8	10.6	27.7	2.8	1100	1225
	Montana US	44.5	20.3	2.2	1.6	15.7	3.5	1125	1205
	Miike Japan	47.7	20.8	2.3	10.2	9.7	1.5	1165	1320
	New Hope Australia	62.5	30.0	2.1	2.6	0.9	0.4	>1450	>1450
	Mafty Russia	60.6	21.9	2.8	5.1	5.0	1.9	1170	1360
	Coal Mountain Canada	39.9	27.3	1.5	2.5	22.1	3.2	1200	1450
	Donbass Ukraine	53.8	20.4	2.6	15.1	2.8	1.3	1150	1370
	RUS	55.6	24.5	2.3	7.2	3.2	0.9	1290	1460
	Colombian	61.8	21.1	2.9	6.6	2.2	2.1	1250	1410
	South African	43.7	34	1.3	3.0	7.2	2.2	1390	1500
	US high Sulfur	43.5	22.6	1.9	21.2	4.0	0.8	1070	1300
	Indonesian	25.6	7.5	3.4	11.2	14.3	4.8	1080	1140
	Polish	46.8	21.8	2.1	9.6	5.8	3.5	1182	1350
	New Hope Australia	62.5	30.0	2.1	2.6	0.9	0.4	>1450	>1450
	Mafty Russia	60.6	21.9	2.8	5.1	5.0	1.9	1170	1360
	Coal Mountain Canada	39.9	27.3	1.5	2.5	22.1	3.2	1200	1450
	Donbass Ukraine	53.8	20.4	2.6	15.1	2.8	1.3	1150	1370
	Russian	55.6	24.5	2.3	7.2	3.2	0.9	1290	1460
	Colombian	61.8	21.1	2.9	6.6	2.2	2.1	1250	1410
	South African	43.7	34.0	1.3	3.0	7.2	2.2	1390	1500
	US high Sulfur	43.5	22.6	1.9	21.2	4.03	0.84	1070	1300
	Indonesian	25.6	7.5	3.4	11.2	14.3	4.8	1080	1140
	Polish	46.8	21.8	2.1	9.6	5.8	3.5	1182	1350
UK Bituminous Coals	L = Low Si	31.4	17.6	1.8	23.2	12.5	0.6	1040	1110
	Low Si	36.8	23.9	1.5	11.2	12.0	2.5	1240	1320
	Low Si	34.3	23.8	1.4	26.3	3.3	0.7	1060	1220
	High Si	47.8	26.8	1.8	16.6	1.3	1.1	*	*
	High Si	47.0	25.5	1.8	14.1	6.4	3.0	*	*
Brown Coals	Greek	31.07	12.85	2.4	7.69	38.92	4.45	1238	1280
	German	1.3	1.5	0.9	18.6	35.8	16.3	1310	1350
	Polish	55.0	24.1	2.3	9.3	3.4	1.5	1250	1480

*Not available.

fouling propensities of fuels. This paper looks, for the first time, at the individual mineral impact on the AFT temperatures and the OAAFT curve. The purpose of this investigation is to reaffirm the impact of individual components on ash fusion temperatures and identify any impact of individual components on the OAAFT curve.

2. Materials and methods

2.1. Ash database

A database (Table 1) was populated using published data on UK bituminous coals and brown coals from the EU [4], Chinese coals and a range of international coals [27]. These coal compositions were collated and used to generate and 'average' coal ash consisting of only SiO_2, Al_2O_3, Fe_2O_3, CaO, and MgO. This study aimed to create baseline profiles in the OAAFT for the most common mineral components found in coals and compare them to their FactSage profiles. Further studies will explore the impact of minerals such as K_2O and Na_2O which also influence ash fusion temperatures [22].

2.2. Synthetic ash samples

The average ash values based on the database (Table 1) were used as a basis to examine the impact of the individual ash compositions with the aim of creating baseline profiles of the main minerals found in coals. Silica-Alumina (S/A) ratio (0.5:1–4:1), and weight percentages of CaO (0–40%), Fe_2O_3 (0–40%) and MgO (0–25%) were investigated. The extremes in variations of individual components were based on previous studies [26,27] and within the range of values for the coals listed in Table 1. The chemical compositions of SiO_2, Al_2O_3, CaO, Fe_2O_3, and MgO for the 20 pseudo ash samples are given in Table 2. The Al_2O_3 (Aluminum oxide, <10 μm avg. part), SiO_2 (Quartz, Sand, White quartz), Fe_2O_3 (Iron(III) oxide, particle size <5 μm, ≥ 99% trace metal basis), CaO (Calcium Oxide, Reagent Grade) and MgO (Magnesium Oxide, −325 Mesh, ≥ 99% trace metal basis) were sourced from Sigma Aldrich. All components were weighed out and added to its respective sample. Each sample was then milled using a pestle and mortar and then ashed at 815 °C using the British standard for coal ashing [38]. All samples were analysed using X-ray fluorescence (XRF) to verify the composition had not changed during this process, as described in Section 2.3. The pseudo pellets were made in a Specac 5 mm pellet press and pressed in an Instron Universal testing system 3360 based on the OAAFT method detailed by Daley et al. [20]. 0.1 g of sample sieve to <75 μm was compressed into a 5 mm pellet at 7500 PSI.

Table 2
Mixing ratios of minerals of the 20 of the pseudo pellets. The percentage of mineral of interest is highlighted in bold.

Composition/wt% (XRF)						
	SiO_2	Al_2O_3	Ratio	Fe_2O_3	CaO	MgO
CaO	54	28	1.9	18	**0**	0
	48	25	2.0	16	**11**	0
	43	22	2.0	14	**20**	0
	37	20	1.9	12	**31**	0
	33	16	2.0	11	**41**	0
Fe2O3	56	29	1.9	**0**	15	0
	51	26	2.0	**10**	13	0
	45	23	2.0	**20**	12	0
	39	20	2.0	**31**	11	0
	33	17	2.0	**41**	9	0
MgO	47	24	2.0	16	13	**0**
	47	24	1.9	16	13	**5**
	47	24	2.0	16	13	**11**
	47	25	1.9	16	12	**18**
	47	24	2.0	16	13	**25**
S/A	**25**	48	0.5	16	12	0
	36	36	1.0	15	13	0
	48	25	1.9	16	12	0
	54	18	3.0	16	12	0
	57	15	3.9	16	12	0

2.3. Fused tablet X-ray fluorescence (XRF)

To obtain elemental data of high enough accuracy for the FactSage analysis, fused tablet XRF was carried out. The ash samples were first ignited at 900 °C to drive off any volatiles, the loss in wt. % is recorded in the table as loss on ignition (LOI). Once ignited, the samples were mixed with a fluxing agent at a ratio of 10:1 (fluxing agent to sample) to reduce the impact of the crystal effects by fused tablets in comparison to powder XRF. The mixture was then heated in a platinum pot with an oxygenated flame. The molten mixture was poured into a mould and air cooled. The fused tablets were analysed using a PANalytical Axios-Advanced XRF spectrometer.

2.4. Ash fusion temperatures and test curves

The OAAFT profiles were obtained using the Carbolite Gero Ash Fusibility Test Furnace - CAF G5. Samples were placed on Carbolite 25 mm × 25 mm recrystalised alumina (RCA) ceramic tiles and loaded in the furnace. The furnace temperature was increased from 25 °C to 1600 °C at a rate of 7 °C/min under oxidising condition (air flowrate of 4 l/min at 27.5 kPa (4 psi)). Images were taken every 1 °C on an integrated HD 1.3 Mb camera with 1280 by 1024 pixel image size. Each sample was performed twice, with the average displayed on the OAAFT plot. Conventional ash fusion tests use hand pressed cones which result in poor repeatability and a delay the response of the IDT [20]. To counter this, the OAAFT was developed a standardised test using pre-milled ash pressed in mechanical press to ensure a repeatable test whilst also giving the best representation of the first point of melting. Details of the development of the OAAFT can be found in a previous study by the authors [20].

MATLAB (version R2017b) was used to analyse each image in a process adapted from work by Pang et a. l [19]. The images are cropped automatically based on the starting location of the sample. The pellet was then automatically tracked during the experiment using a combination of edge detection and thresholding techniques. Five thresholding techniques were used in total including Canny [39], Otsu [40], Prewitt [41], Bradley Adaptive Thresholding [42], and Log methods [39]. These techniques were chosen based on the different image histograms obtained at different points in the test. Canny [39] and Otsu [40] were both suited to the early test back-lit range of images (0–500 °C). Prewitt was used in the transition where the back light turns off and the radiative light begins (500–800 °C). Finally, the Bradley [42] and log methods [39] were better suited to the end test images (800–1600 °C). These techniques are used to create a pellet outline. This outline was then used to capture the height and centroid parameter of the pellet. The centroid was used to track the location of the sample and the height was compared to the initial height of the pellet to plot relative height.

2.5. Slagging and fouling indicators

Based on the contained oxides of the ashes, the base-to-acid ratio (B/A) can be calculated (Eq. (1)) [43]. B/A has displayed the tendency of oxides to act as oxygen donator/network modifier (base) or as an oxygen acceptor/network former (acid) similar to the chemical definition of bases and acids from Brønsted [44]:

$$\frac{B}{A} = \frac{CaO + MgO + K_2O + Na_2O + Fe_2O_3}{SiO_2 + Al_2O_3 + TiO_2 + P_2O_5} \quad (1)$$

This equation can be reduced for the 5 elements in the pseudo pellets:

$$B \Big/ A = \frac{CaO + MgO + Fe_2O_3}{SiO_2 + Al_2O_3} \quad (2)$$

The B/A ratio gives an indication of the potential melting-point of

coal ash on combustion particularly in the secondary superheater and economiser tubes [45]. Such fouling deposits impede gas flows and dramatically reduce efficiency and are related according to the equation. The B/A ratio is known to influence fusion behaviour [44,46]. Acidic ash systems are mainly dominated by the high melting temperatures of aluminosilicates and clearly basic ashes are defined by the high melting temperatures of CaO and MgO [47,48]. Ashes with intermediate B/A values (B/A≈0.7–1.0) have typically produced the lowest ash fusion temperatures [46]. The slagging tendency of the ash increases with increasing B/A ratio. The ash is expected to have low slagging inclination when B/A < 0.5, medium for 0.5 < B/A < 1, high for 1 < B/A < 1.75 and severe for B/A above 1.75, based on mass fraction of each oxide in the ash (wt%) [49]. The iron/calcium (I/C) ratio (eq. (3)) takes into account the ferric oxide (Fe_2O_3) portion of iron [50]. Normally, lower I/C ratios tend to lower the ash-softening temperature.

$$\frac{I}{C}=\frac{Fe_2O_3}{CaO} \tag{3}$$

The Slag viscosity index or Silica ratio (Sr) in Eq. (4) is used to evaluate the slagging tendency inside the furnace [49]. High values correspond to high viscosity and therefore low slagging. Low slagging occurs when Sr is above 72, medium for 65 < Sr < 72 and high for values below 65.

$$Sr=\left(\frac{SiO_2}{SiO_2+CaO+MgO+Fe_2O_3}\right)\cdot 100 \tag{4}$$

2.6. Thermochemical calculations

The fusion behaviour of the ashes is produced with aid of the thermochemical software package FactSage™ applying the version 7.2 [51]. Herein, the chemical equilibrium is calculated by a minimization of the Gibbs free energy. For this purpose, the databases of FToxid, FTmisc, FTsalt, and FactPS are used in that specific order [48]. A selection of solution phases has comprised A-Slag, A-Spinel, A-Monoxide, and Mullite (each with the option of two immiscible phases) due to the simple ash system. The composition of the ashes (Table 2) was used as input data by the respective amounts in gram (in total about 100–125 g). An air atmosphere of 2000 g (composed by the main species of 1511.24 g N_2, 462.98 g O_2, and 25.78 g Ar) and a total pressure of 1 atm is employed according to the ash fusion test [48]. In principle, different ratios of the atmosphere to the solid ash species in a range from 10:1 to 500:1 have demonstrated a minor impact on the mineral phase composition [46]. For reason of comparability, all calculations are performed from 800 to 1600 °C with a step size of 20 °C. Such kind of calculation is applied for comparison to experimental ash fusion behaviour by various authors [52–55]. In the experiment several effects occur, which cannot be reproduced by the thermochemical calculation [46,48]: (1) For example, the formation of mineral phases are aggravated by kinetic limitations, transport restrictions, and unknown reactions. (2) The thermochemical calculations suppose an ideal mixing of all species, but in reality, particle-related effects, e.g. interfaces, limited mass transport, and unreactive/marginally reactive species (like quartz grains) may appear. (3) Aluminosilicates tend to form glassy solids, which is not reflected by the FactSage™ calculation in comparable way.

3. Results and discussions

3.1. Pseudo pellet individual mineral analysis

A pellet was formed of each of the individual minerals (MgO, CaO, Al_2O_3, and Fe_2O_3) and heated in the OAAFT oven. It was not possible to make a pellet of SiO_2 due to SiO_2 being composed of spherical particles which couldn't be pressed into pellets. During the AFT test in the CAF oven, the shape of each pellet was recorded and then subsequently analysed. As illustrated in Fig. 1, a typical AFT test involves a pellet going through shrinkage, deformation, hemisphere and flow stages, which can be measured quantitatively via image analysis and related back to the temperature at which these changes occurred [20]. The "*OAAFT Parameter*" was used to assess the combined shrinkage, deformation, and curvature of the pellets during the tests based on the image analysis results. Equations (5)–(7) were used to calculate the percentage shrinkage (S), initial deformation (ID), and curve shape (CS). The area (A) of the pellet was defined as the area of the 2D cylinder and was measured by tracking the centroid of the shape. The perimeter (P) is the length of the continuous line forming the boundary of the closed pellet shape. Eccentricity (E) is defined as the ratio between the distance between the foci of the ellipse (F) and its major axis length (l). The foci are defined as square root ($F=\sqrt{a^2-b^2}/(a+b)$ with major radius a and minor radius b) and has a value between 0 and 1. An ellipse whose eccentricity is 0 is a circle, while an ellipse whose eccentricity is 1 is a line segment. The axial ratio is the ratio of the minimum and maximum length (in pixels) of the mirror axis of the ellipse that has the same normalised second central moment as the region. Aspect ratio (AR) is the ratio of the height of the bounding box and the width of the bounding box surrounding the cylinder. The data for the three variables were then concentrated in an array in Matlab using the cat function to produce the "*OAAFT Parameter*".

$$S = A^{\frac{1}{2}}*(4P)^2$$

$$\%\ S=\frac{S_{T_o}}{S_T} \tag{5}$$

$$ID=A_0*E*AR$$

$$\%\ ID=\frac{ID_{T_o}}{ID_T} \tag{6}$$

$$CS=A*AR$$

$$\%\ CS=\frac{CS_{T_o}}{CS_T} \tag{7}$$

Where S_{T_o} is initial shrinkage, S_T is shrinkage at time T, ID_{T_o} is initial deformation, ID_T is deformation at time T, CS_{T_o} is initial curve shape, CS_T is the curve shape at time T, and A_0 is initial area. The resultant individual mineral curves are shown in Fig. 2, with the average result denoted by the solid line with a coloured error band above and below. The following trends were noted per mineral:

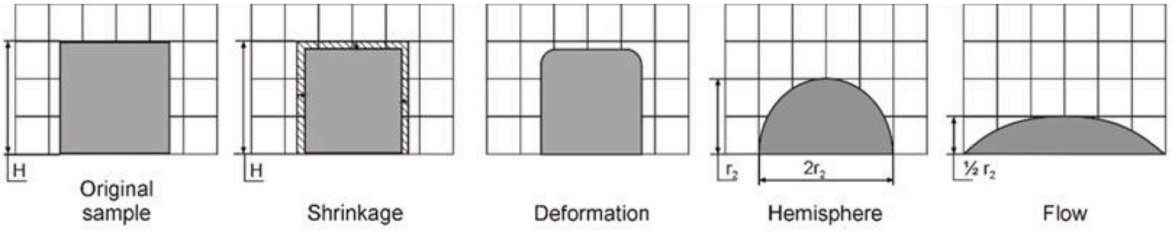

Fig. 1. AFT shape progression for pellet.

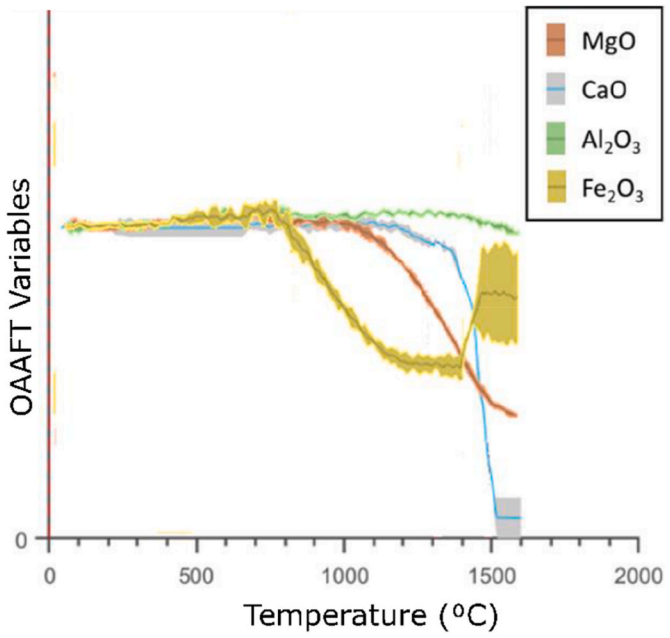

Fig. 2. Individual mineral curves from the OAAFT. Average data of two runs is shown as a solid line for each mineral, with a coloured error band denoting the error in the results.

- CaO: Calcium oxide is the only component that reaches Fluid Temperature (FT) at 1500 °C. There is only a marginal shrinkage period of around 5–10%. The low melting temperature could be a result of $CaCO_3$ forming due to contact with atmospheric CO_2 [56]. The melting point of $CaCO_3$ is 825 °C [57], while pure CaO is 2575 °C.
- Fe_2O_3: The iron oxide curve displays clear shrinking properties for a sharp increase. This is similar to many traditional coal ashes and is likely to be the component responsible for this behaviour.
- MgO: The magnesium oxide curve reaches the end of the test without completion of the S-type shape. It is likely that the reduction shown is shrinkage before a further deformation phase based on the change in gradient between 1500 and 1600 °C.
- Al_2O_3: Aluminium shows very little change over the studied range 0–1600 °C, a very small level of shrinkage, around 1–5%, at around 1450 to 1600 °C.

The analysis of the individual mineral curves in the OAAFT demonstrates that they all have very different behaviours during heating. To gain a greater understanding of the impact of each mineral on the AFT, their ratios were varied as detailed in Table 2 and the OAAFT was carried out on duplicate pellets of each.

3.2. Pseudo pellet analysis

20 pseudo pellets with varying quantities of Silica-Alumina (S/A) ratio (0.5:1–4:1), and weight percentages of CaO (0–40%), Fe_2O_3 (0–40%) and MgO (0–25%) were investigated in the OAAFT. The aim was to ascertain the impact of each mineral on the OAAFT profile and ash fusion temperatures. Table 3 details the key figures of Base-to-Acid (B/A) ratio, Iron–Calcium (I/C) ratio, silica content, and characteristic temperatures of the ash fusion IDT and FT for the 20 of the pseudo pellets. Ash fusion temperatures (IDT and FT) are highest for 0% mineral addition (without addition of basic oxides of CaO, Fe_2O_3, and MgO). As the percentage of mineral addition increases, the IDT and FT decreases, which agrees with literature [26]. As noted in previous studies, the ash fusion temperatures increase after around 30% for Fe_2O_3 and MgO. This is also observed with CaO concentrations above 38% in the ash network [58]. Varying S/A ratios had no impact on the B/A ratio, which indicates

Table 3
Key figures of the base-to-acid (B/A) ratio, Iron–Calcium (I/C) ratio, silica content, and IDT and FT temperatures of the 20 of the pseudo pellets. Standard deviation of runs provided for IDT and FT temperatures.

	Percentage of Mineral addition (wt%/ratio)	B/A ratio	I/C ratio	Silica content (%)	AFTs (°C)	
					IDT	FT
CaO	0	0.22	0.0	75	1461 ± 1	1539 ± 1
	10	0.37	1.5	64	1320 ± 1	1363 ± 13
	20	0.53	0.7	56	1353 ± 4	1385 ± 1
	30	0.76	0.4	46	1308 ± 4	1344 ± 1
	40	1.05	0.3	39	1266 ± 4	1296 ± 5
Fe_2O_3	0	0.17	0.0	79	1404 ± 26	1482 ± 3
	10	0.30	0.8	69	1329 ± 1	1399 ± 0
	20	0.48	1.7	58	1300 ± 6	1359 ± 4
	30	0.71	2.9	48	1307 ± 5	1356 ± 0
	40	0.98	4.5	40	1330 ± 3	1386 ± 1
MgO	0	0.40	1.3	62	1306 ± 2	1365 ± 4
	5	0.47	1.3	58	1298 ± 3	1321 ± 0
	10	0.55	1.3	55	1225 ± 7	1292 ± 1
	20	0.64	1.3	51	1211 ± 6	1251 ± 1
	30	0.76	1.2	47	1255 ± 1	1286 ± 4
S/A	0.5:1	0.39	1.3	47	1402 ± 1	1452 ± 1
	1:1	0.40	1.2	56	1353 ± 2	1405 ± 3
	2:1	0.39	1.3	63	1308 ± 4	1362 ± 1
	3:1	0.39	1.3	66	1226 ± 6	1346 ± 6
	4:1	0.39	1.3	67	1189 ± 0	1321 ± 12

that the fouling tendency of the fuel ash is unaffected by the S/A ratio. S/A is a key factor in slagging and sintering in boilers [28]. Ash with higher S/A ratios have a higher viscosity liquid phase and can be considered a Newtonian fluid at FT when the S/A is above 3.5 due to the low solid content. The B/A ratio increased for all other samples as the percentage of mineral increased. Intensive slagging has been noted when the B/A ratio is between 0.75 and 2 [59], which was seen in this study when CaO, MgO and Fe_2O_3 are over 30% (Table 3). As expected, the I/C ratios remained virtually constant for varying MgO and S/A as the CaO and Fe_2O_3 contents were fixed for these samples. Silica content reduces for all minerals as their percentage increases apart for S/A. The next section of this study explores the individual OAAFT profiles for each mineral in turn to identify key trends and behaviours.

3.2.1. CaO comparisons

The CaO content was varied between 0% and 40% in this study to encompass the range of CaO in international fuels taken from literature (Table 1). Along with Fe_2O_3, CaO is one of the main fluxing agent which reduce the AFTs of coal ashes [15,23,60]. This is supported by the data in Fig. 3, up to 30%. There is rapid decrease (20 °C/wt%.) in AFTs (~200 °C) between 0 and 10% CaO. Once this effect has occurred there is a plateau between 10% and 40% where the AFTs generally decrease (3.3 °C/wt%) but only by 100 °C. As the other data sets pass 40%, the AFTs begin to in increase again at a similar rate. There are discrepancies

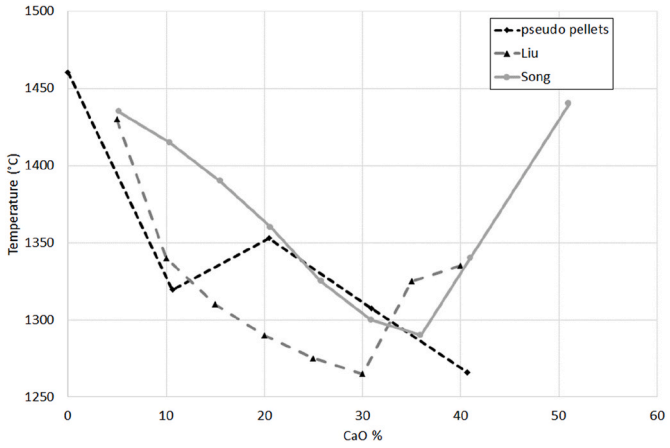

Fig. 3. Comparison of pseudo pellet deformation temperatures of CaO variation with existing literature.

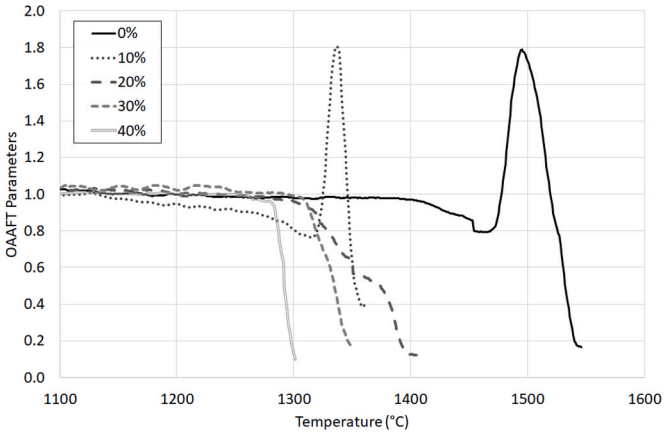

Fig. 4. OAAFT curves for the CaO-enriched pseudo pellets ranging from 0 to 40% weight (S/A = 2.0).

in the data, as the OAAFT shows no minimum point, while the studies by Lui et al. [27] and Song et al. [26] have minima at 30 and 35% respectively then rise. Lui's [27] explanation for the rapid reduction in the AFTs followed by a rapid increase as the CaO ratio increase over 40%, as noted in Fig. 3, has been attributed to low melting eutectics of CaO with other minerals, whilst at higher concentrations high melting CaO monomer forms to raise the AFTs [27]. The lack in rapid increase in AFT for the OAAFT in this study could be related to the use of high-pressure pellets enabling eutectics at higher concentrations.

It should be noted that there are only a few traces of other network transformers in the pseudo pellets used in this study. In contrast, all other studies using these species as additives to modify the ash behaviour have them present in the initial ashes. The characteristics of the ash components (including the liquid slag) can be described via network theory, where a SiO_2 network is interrupted by alkaline and earth alkaline metals [46]. The stability of this network depends mainly on the ratio of network formers and network transformers. This can be expressed by the base to acid ratio (B/A), which can further be related to ash fusion temperatures (Table 3). This ratio has been derived from a network of tetrahedral silicates, where two silicon atoms are connected by an oxygen atom [61]. Acidic oxides, such as SiO_2, TiO_2, and partially amphoteric oxides (Al_2O_3 and Fe_2O_3), are network formers due to oxygen acceptance and occupation of tetrahedral network positions. Basic oxides, such as Na_2O, K_2O, CaO, and MgO, are network transformers as these act as terminal groups in a silicate network. The B/A ratio is not discussed in the studies by Lui [27] and Song [26]. In this study, intensive slagging was been noted when CaO exceeded 30%, which is known to occur when the B/A ratio is between 0.75 and 2 [59].

Song [26] observed a shift in sub-liquidous phase from low-temperature melting gehlenite to high-temperature melting mullite at 5–35% CaO, which shifted back again when the CaO ratio increased from 35 to 40%. Song [26] conducted their study in an Ar atmosphere and Liu [27] conducted their study in a carbon atmosphere, while this study was conducted in atmospheric conditions. The atmospheric conditions used in this study appear to have impacted these results. The reducing conditions have shifted the late increase in deformation temperature to 30%, whereas the inert conditions show the shift at 35%, while the oxidising environment does not show the phenomena at all. Furthermore, the AFTs under reducing atmosphere are generally around 50–100 °C lower than that of the oxidising conditions. Further studies will examine the influence of reducing atmospheres on AFTs in the OAFFT.

The OAAFT curve in Fig. 4 for the CaO pseudo pellets indicate that the pseudo pellets go through a drastic transformation from 0 to 40% CaO. The difference between IDT and FT (sometime denoted as ash fusion interval) continuously shrinks as the percentage of CaO is increased. At 0% the difference is nearly 100 °C, and by 40% the difference is down to 25 °C. The addition of CaO reduces the shrinkage of the samples, and thus there is no sign of sintering before IDT. The most obvious change that can be seen is the loss of the expanding phase completely from the curve. The closest example of the raw CaO curve is the 40% weight sample, and this is to be expected with the highest concentration of CaO. Nonetheless, a domination of the ash fusion behaviour is detected for additions >38% CaO [58]. The only difference is that the IDT comes at around 100 °C earlier.

3.2.2. Fe_2O_3 comparisons

Iron occurs in coal mainly as ferric iron in both oxidising and inert conditions, but as ferrous iron or even metallic iron under reductive atmospheres [27,62]. The Fe_2O_3 studied in this investigation ranges from 0 to 40% based on the range in coal ashes in Table 1 (section 2.1). The comparisons of the two studies in literature [26,27] and the AFT of Fe_2O_3 in the OAAFT are displayed in Fig. 5 and show good correlation in trends of the IDT. The OAAFT IDT decreases as CaO increases from 0 to 30%, with the minimum being 100 °C and maximum being 275 °C. Liu et al. [27] does not analyse the impact of Fe_2O_3 above 30%, however this study and that of Song [26] continue up to 40% which show a slight increase in IDT. The greatest impact on IDT is seen between 0 and 20% Fe_2O_3, and as the Fe_2O_3 composition increases, the trend in IDT levels off.

Whereas the CaO investigation displayed an earlier local minimum under reducing atmosphere increasing to inert and then oxidising (Fig. 3), the Fe_2O_3 study shows the opposite trend. Both this study and

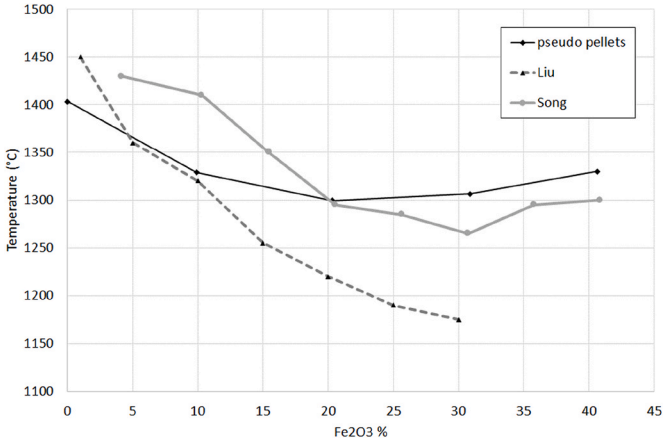

Fig. 5. Comparison of pseudo pellet deformation temperatures of Fe_2O_3 variation with existing literature.

the study by Song [26] exhibit a parabolic curve, with the minima around 20% Fe_2O_3 for this study and at around 30% Fe_2O_3 for an inert atmosphere in Song's study. In contrast, the carbon atmosphere (Liu [27]) has not yet reached its minimum point, indicating that atmosphere once more plays a role in the IDT values of the ash. Similar to the CaO investigation, the reducing AFTs are lower than the oxidising AFT values, but are more consistently around 100 °C less. The general trends in AFTs in the reducing investigation can be attributed to an increase in FeO rather than Fe_2O_3. This is due to new chemical bonds forming between Fe(II) and unsaturated oxygen and subsequent eutectic compounds between the FeO and other oxides at high temperatures [27]. It might explain the shift in this trend, whereby oxygen is more readily available and stems the increase in FeO. Fe is more likely to cause slagging in a reducing atmosphere [27]. Thus, the study emphasises the role of ferric and ferrous iron in the slagging and fouling of ashes and how atmospheric conditions can influence the results.

The comparison of the individual components in Fig. 2 identified Fe_2O_3 as the component with greatest and earliest change in the ash network. This is reflected in Fig. 6, as the addition of Fe_2O_3 has an instant impact on the shape of the OAAFT curve. The addition of iron initiates a shrinking and expanding phase. All the samples containing Fe_2O_3 shrink by 20–40% and from the sintered size all samples appear to at least double in size, which is in remarkable contrast to CaO. When the CaO concentration increases it depresses and finally removes the peak from the curve, it seems that the iron in the sample is either responsible for the expanding phase or, at the very least, does not inhibit it. The AFT range stays constant throughout all the samples, suggesting that Fe_2O_3 has a low impact.

3.2.3. MgO comparison

Magnesium oxide (MgO) is a minor component to most coal ashes. However, it is a basic oxide and even at low concentrations can impact melting characteristics [26]. Increasing the concentration can lead to lower AFTs and prove beneficial to flow properties of coal ash slag samples [26,63]. In this study, five pseudo ash pellets were created to cover the range of MgO (0–30 wt% – Table 1) whilst reflecting the compositions of the range of coal ashes from Table 1. The IDT of the samples were then plotted and compared to the results of Song study [26] which also looked at the impact of MgO (Fig. 7). Song's results do not match exactly with the findings from this study, however they display a general decrease from 0 to 15% of around 100 °C. The results reflect a similar behaviour to iron, a minimum point at 20% weight with increasing IDTs either side. MgO belongs to the alkaline earth metals which are classed as network modifiers [64]. MgO has the ability to modify the alumina network structure as well as the silicate network sturcture in a similar way to CaO and promote crystal precipitation.

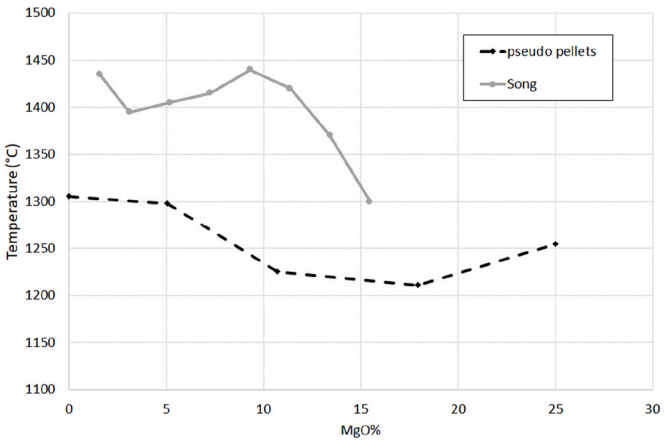

Fig. 7. Comparison of pseudo pellet deformation temperatures of MgO variation with existing literature.

Synergistic effects have been noted between CaO and MgO on ash fusion characteristics in a reducing atmosphere [65]. Low CaO/MgO ratios result in the formation of spinel with stable lattice resulting in higher AFTs, while higher CaO/MgO ratios lead to the formation of low-melting point fieldspar minerals which result in reduced AFTs. This aligns with the results of this study and Song's [26]. Once more, the variance in the results in likely to be related to the variance in atmospheres, with Song's being inert and this study being atmospheric.

As shown in Fig. 8 when the MgO is increased the OAAFT curve changes in shape similarly to that of the CaO OAAFT but with increased potency. The expansion phase is completely lost with only 5 wt% addition of MgO added and the AFT range is reduced by half. The sintering phase is sustained until 10 wt% addition. Unlike CaO, which trends towards is individual component curve shape, the MgO curves tend towards the CaO curve shape with no sintering and minimal AFT range. The exception to this is that at 30% MgO the expansion phase returns and the sample expands by 20% after the IDT.

3.2.4. Silica-Alumina (S/A) ratio

The S/A ratio is known to play an important role in AFTs and ash melting properties [66]. Al_2O_3 acts as a 'support skeleton' that inhibits the deformation of the ash, while SiO_2 forms low melting point eutectics with basic oxides [67]. Thus, increasing S/A ratio promotes slagging. In this study five pseudo ash pellets were created to cover the range of S/A ratios (0.5–4 –Table 1) whilst reflecting the compositions of the range of coal ashes from Table 1. The DT of the samples were then plotted and compared to current literature in Fig. 9. In addition to Liu and Song's

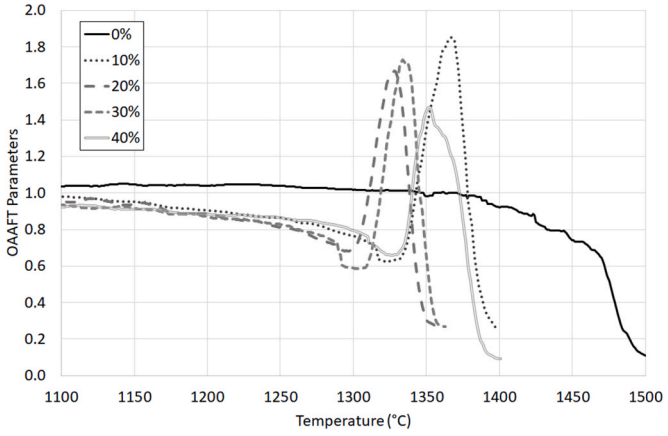

Fig. 6. OAAFT curves for the Fe_2O_3-enriched pseudo pellets ranging from 0 to 40% weight (S/A = 2.0).

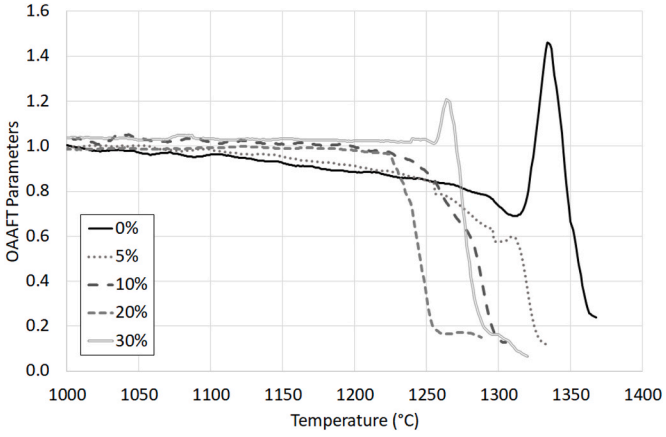

Fig. 8. OAAFT curves for the pseudo pellets ranging from MgO of 0–30% (S/A = 2.0).

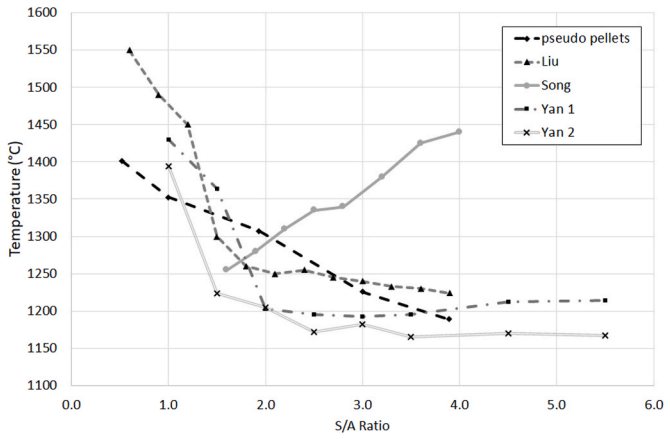

Fig. 9. Comparison of pseudo pellet deformation temperatures of S/A variation with existing literature.

studies [26,27], two groups of samples in a study by Yan [28] are also included. Yan investigated two groups of samples where the CaO had been increased from 16% (Yan 2) to 23% (Yan 1) to shift the B/A ratio. Yan's study was conducted in an Ar (inert) atmosphere.

All the investigations have slightly differing components in each of their pseudo pellets [26–28], which is due to the coals that they are attempting to reflect. This has the impact of causing slightly varying trends. In most cases however, increasing the S/A ratio results in reducing the IDT. It is difficult to explain the results found by Song [26], as they are clear outliers compared to other studies, especially as Yan's [28] study was also conducted in a Ar atmosphere. The only difference in Song's study is that it includes minor constituents, MgO, TiO_2, Na_2O and K_2O in all samples in relatively small quantities. The other investigations only add MgO and K_2O into specific tests to identify the impact of each individual component. These minor constituents may have cumulatively impacted on the overall eutectics of the mixture [68]. Three of the studies identified a steep drop of roughly 200 °C in DT between an S/A of 1 and 2 before a plateau an S/A over 2. Further increasing the S/A has no effect on DT. The trend found using the OAAFT shows a linear decrease in AFTs. As this study was the only one conducted in an oxidising environment, this may have elongated the general trend seen by shifting the plateau, something that has been seen in the other individual component studies. The impact of varying atmosphere on the OAAFT should be investigated in the near future.

The S/A ratio clearly has a large impact on both the shape of the OAAFT curve (Fig. 10) and the AFT temperature range. The most obvious change is that increasing the ratio firstly adds an expansion and sintering phase, and then increases the magnitude of the expansion phase. The expansion increases from 0 to 60% from 1:1 to 2:1, and another 60% to 3:1. The 1:1 sample displays no sintering phase, whilst the 2:1 sample shrinks by 40%. This would suggest that the sintering strength of the samples increases with S/A ratio as seen in the shape of the curve. An increase in AFT temperature range, where a high IDT and low FT are present, can present a severe problem for boiler operation, as a small change in process temperature will result in a shift from solid ash to an entirely liquid. The pulverized coal boilers should operate under the fuel IDT to prevent ash deposits in the heat exchange regions, whilst gasifiers need to operate over their fuel FT to maintain continuous slag flow on gasifier wall [69].

3.3. FactSage comparison

This section covers the FactSage modelling and comparison of the results to the OAAFT test. Figs. 11–14 compare the FactSage modelling of slag formation to the OAAFT for the pseudo pellets. Table 4 summarises the FactSage predicted slag formation onset temperatures and OAAFT ash fusion temperatures for the pseudo pellets. The general trend for all the minerals is that increasing each mineral content will decrease the slag formation onset temperature, but the amount will vary by mineral. S/A and CaO have the largest reduction in slag formation onset temperature, with reductions of 180 °C [26,68,70]. In contrast Fe_2O_3 reduces the onset temperature by around 80 °C.

The notable results for each component are summarised as follows:

- *CaO (Fig. 11):* In Fig. 11, as CaO content increases slag formation onset temperature decreases, which indicates the role of CaO as a strong network transformer [26,68,70]. Without CaO addition, the slag formation starts around 1400 °C, but decreases to 1220 °C for 30% and 40% CaO. At 20% CaO, there is a slight increase in IDT and FT, and slag formation onset temperature drops to 1160 °C, and has been noted in previous studies [26,68,70]. The OAAFT profile changes with varying CaO content reflect those of the FactSage modelling.
- *Fe_2O_3 (Fig. 12):* At increasing Fe_2O_3 content (Fig. 12), the slag formation onset temperature decreases, but only by 80 °C [68]. At 0% Fe_2O_3 the slag formation onset temperature is 1380 °C, but for all percentages of Fe_2O_3 the slag formation onset temperature is 1300 °C. At 30%, there is a drop in the slag formation onset temperature to 1160 °C compared to the neighbouring Fe_2O_3 percentages, which has also been noted in previous studies [26,68,70]. There is good alignment of the slag formation onset temperatures for Fe_2O_3 and the onset of ash fusion in the OAAFT profiles. Thus, Fe_2O_3 acts as a weak network transformer [68].
- *MgO (Fig. 13):* In Fig. 13, as MgO content increases slag formation onset temperature decreases. The slag formation onset temperature

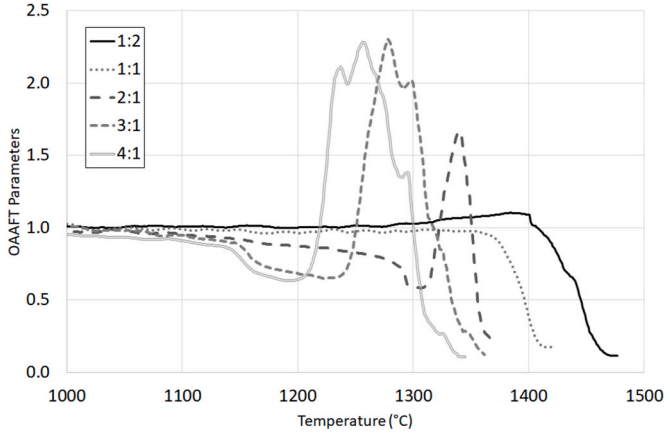

Fig. 10. OAAFT curves for the pseudo pellets ranging from S/A of 0.5:1–4:1.

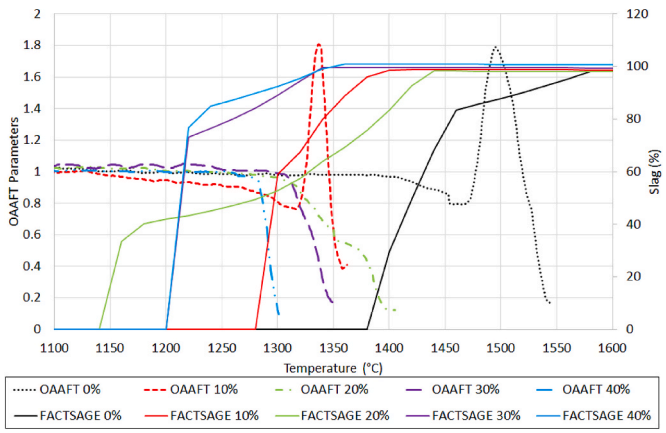

Fig. 11. CaO OAAFT and FactSage comparison.

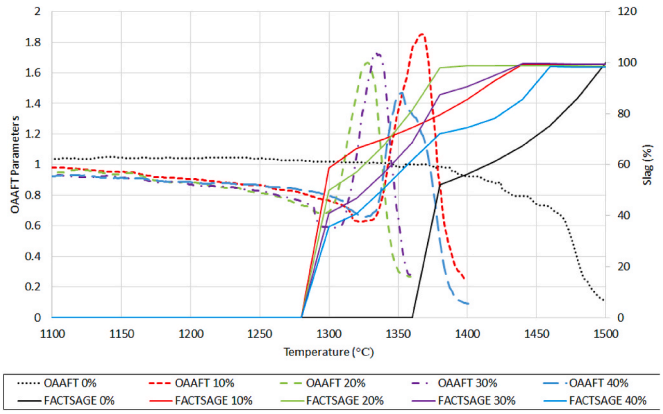

Fig. 12. Fe_2O_3 OAAFT and FactSage comparison.

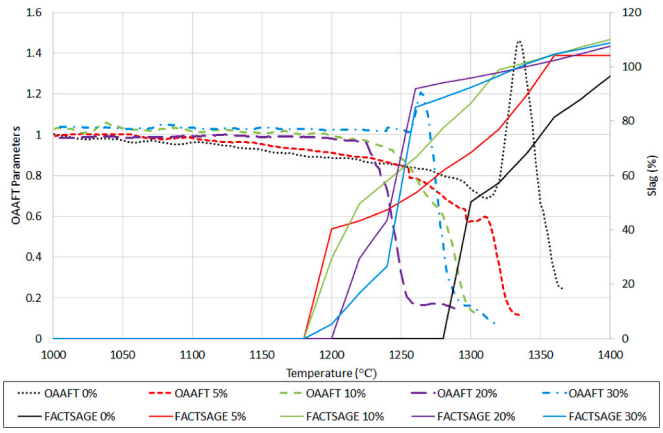

Fig. 13. MgO OAAFT and FactSage comparison.

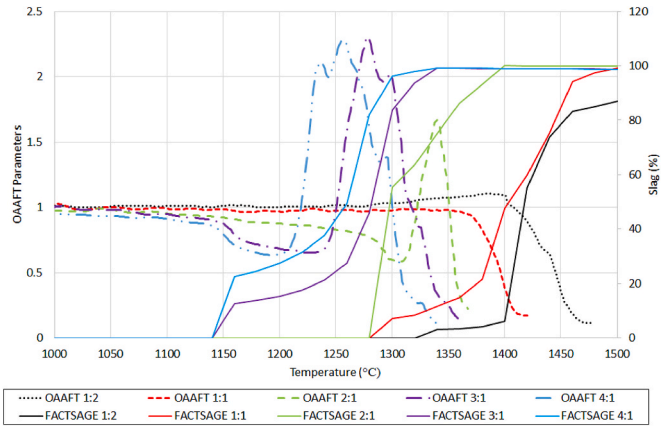

Fig. 14. S/A ratio OAAFT and FactSage comparison.

is 1300 °C with no MgO addition, and drops to 1200 °C for all MgO percentages. At 20%, the slag formation onset temperature increases slightly to 1220 °C, but reduces back to 1200 °C at 30% MgO. There is good alignment of the slag formation onset temperatures for MgO and the onset of ash fusion in the OAAFT profiles. The effect of MgO in the ash can be evaluated as a moderate network transformer.

- *S/A Ratio (Fig. 14):* As the S/A ratio increases in Fig. 14, the slag formation onset temperature decreases. The onset temperature decreases from 1340 °C for S/A 1:2 ratio to 1300 °C for S/A ratios of 1:1 and 2:1, and then to 1160 °C for S/A ratios of 3:1 and 4:1. This is the biggest reduction in slag formation onset temperature for all the minerals analysed. Again, there is good agreement between the slag formation onset temperatures for S/A and the onset of ash fusion in the OAAFT profiles. This kind of ash system can be well described by the FactSage calculations.

Table 4
FactSage predicted slag formation onset temperatures and oaaft ash fusion temperatures for the pseudo pellets.

	Percentage Mineral (%/ratio)	Slag Formation Onset Temperature	AFTs (°C)	
			IDT	FT
CaO	0	1400	1461	1539
	10	1300	1320	1363
	20	1160	1353	1385
	30	1220	1308	1344
	40	1220	1266	1296
Fe_2O_3	0	1380	1404	1482
	10	1300	1329	1399
	20	1300	1300	1359
	30	1160	1307	1356
	40	1300	1330	1386
MgO	0	1300	1306	1365
	5	1200	1298	1321
	10	1200	1225	1292
	20	1220	1211	1251
	30	1200	1255	1286
S/A	0.5:1	1340	1402	1452
	1:1	1300	1353	1405
	2:1	1300	1308	1362
	3:1	1160	1226	1346
	4:1	1160	1189	1321

A comparison between the lowest calculated temperature with a significant slag level and the experimentally determined initial deformation temperature (IDT) is illustrated in Fig. 15. This temperature point is defined by a calculated mass ≥20 wt% of slag, which was achieved from comparison to the experiment comparable to Ref. [55]. Most samples are found within a range of ±30 °C, which confirms that the presence of at least 20 wt% of liquid slag in the ash system is mandatory to achieve the characteristic point of IDT in the ash fusion test. It should be noted that these results are obtained for pseudo pellets that are shaped by a five-component ash system, which is a simpler system than a real ash. Here, the base-to-acid ratio (B/A, calculate on the mass basis) – according to Eq. 2 – is used as a reference basis for an analysis of the

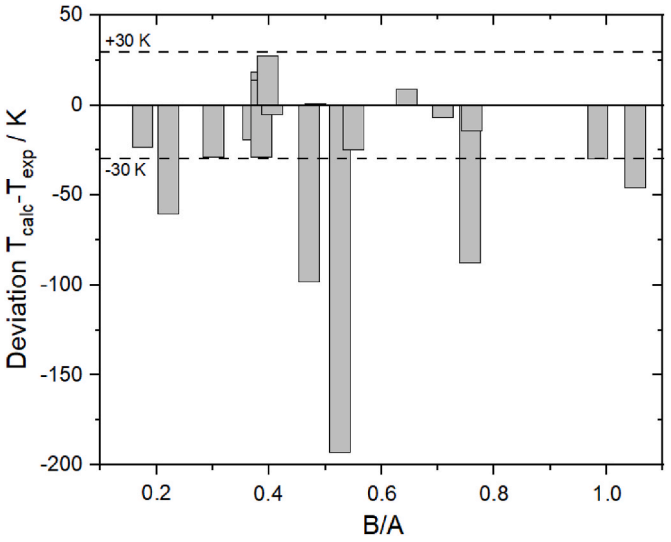

Fig. 15. Comparison between lowest calculated temperature (T_{calc}) with the presence of a significant slag amount (≥20 wt%) and experimentally determined initial deformation temperature (T_{exp}) in relation to the base-to-acid ratio (B/A, calculated on a mass basis).

potential deviations between both. This ratio originates from glass theory and contains a distinction of the oxides into network formers (e.g. SiO_2, Al_2O_3, TiO_2) and network modifiers (e.g. CaO, MgO, Na_2O, and K_2O) characterizing their tendency to reinforce or weaken a glassy network [44].

There is good agreement between calculated and measured temperatures in Fig. 15. For most of the samples, the deviations between calculated and measured temperatures are detected within a bandwidth of ±30 °C, but for some samples higher deviations are apparent. In particular, for low and high B/A values in Fig. 15 the simulated results are in accordance with the experimental results. Those samples are determined either by a high content of high temperature melting mineral phases, e.g. pure quartz and/or alumina-rich silicates, in case of low B/A or the addition of sufficient amounts network modifiers leading to the formation of medium temperature melting minerals, e.g. silicates incorporating alkaline earth oxides, for B/A≈1 [47]. The deviations predominantly exhibit a negative sign, which means that the assumed 'ideal' conditions in FactSage™ are not fulfilled in all pseudo pellets. This results to a fractional melting of the components and higher ash fusion temperatures compared to the samples with an ideal mixture [43]. For ashes with a strong deviation between experiment and modelling, these ashes have contained a sufficient share of basic components with different mixtures of Fe_2O_3 and CaO, while the observed differences may result from synergistic effects [68,71]. In the range of compositions accompanied by critically low onset temperatures for the slag formation with B/A≈0.7–1.0, the good agreement between OAAFT and FactSage indicates a suitable prediction quality of the thermochemical modelling. However, particle-particle interactions will play a more important role in pseudo pellets, as these are composed by artificially blended minerals, which have not preformed previous mineral reactions compared to coal or biomass ashes, where the species are already associated and have initially reacted with each other in the feedstock.

3.4. Relevance of study

The significance of the OAAFT curves responding to changes in individual elements means that it can potentially be used to highlight 'problem' cases. The profiles appear to 'fingerprint' the behaviour of the different components. This fingerprinting is a novel feature of the OAAFT which cannot be provided by the conventional ash fusion test. This study has shown that the fingerprint can be broken down into its major components, and the influence of varying the quantities of these components can be investigated. Furthermore, should a problem arise regarding swelling or sintering the OAAFT could be used to test if mineral additives, such as CaO and MgO, will work to modify the behaviour. This study provides a baseline of how major minerals influence the OAAFT curves, and further research into the influence of less common but influential minerals such as K_2O and Na_2O [22] will help develop a fuller and more detailed model of how minerals influence the OAFFT fingerprints. The FactSage modelling results have supported its predictive capabilities for coal liquidous temperatures alongside the OAAFT. Combining the OAAFT and FactSage results enables a more holistic picture of slagging and fouling tendencies to be drawn. This will enable power generators to better tackle operational issues with combining multiple fuels or using novel fuels such as refuse derived fuels, which have much more complex and varying compositions compared to coals [72]. The OAAFT not only produces highly repeatable ash fusion temperatures, but the characteristic curve profile has been shown to indicate higher or lower elemental concentrations. These could be used as an indicator for further testing, however further work is required to validate the trends.

It was noted that the some of the results deviate from other findings in literature. A factor that could explain these differences would be the ratio of the other elements to the ones of interest (i.e., if CaO is the focus the ratio of components Fe_2O_3, SiO_2, Al_2O_3, and MgO) as well as the transformation of the ash network by various basic components and the potential synergy effects between these components have to be taken into account. An alternative way to compare the results would be to model the samples using FactSage, in the same way that Song investigates [26]. Thus, it would be preferable to compare the closeness of the results to a thermodynamics package such as FactSage instead of directly comparing the AFTs of each study. This would give a reference point which considers the entirety of each sample whilst further validating the package. A similar investigation including K_2O and Na_2O would be an interesting addition as potassium is known to have a strong impact on the AFTs, as these basic oxides work as the network modifiers and form low melting point minerals to drop AFTs and improve the fusibility [22]. Further research is being conducted on how the OAAFT developed for the pseudo pellets is replicated in naturally occurring coal and biomass ashes. In addition, an investigation could also use a standard coal and biomass ash to which individual components are added to identify the impact of raw CaO, Fe_2O_3 etc. on a naturally occurring samples OAAFT.

4. Conclusions

The ash fusion temperatures and OAAFT curves have been measured for a set of pseudo ash pellets based on a range of 31 international coals from literature simplified to a four-component system of SiO2, Al2O3, CaO, and Fe2O3, with a five-component system including MgO. Each component oxide was studied to show its effect on the AFT temperatures and OAAFT curves.

The OAAFT produces a "fingerprint" of a fuel which can be broken down into its major constituent parts. Individual minerals play different roles in the slagging and fouling process. As CaO increases, the AFT range halves, while the addition of Fe_2O_3 initiates a 30–40% shrinkage during the sintering phase and an expansion phase that doubles in size from the sintered size. Increasing the S/A ratio adds an expansion phase which then doubles over the range, while increasing MgO by only 5% weight results in a complete loss of the expansion phase. This study provides a baseline of how major minerals influence the OAAFT curves, and future studies will explore the influence of other minerals and different atmospheres on ash fusion behaviour.

By combining the FactSage data with the OAAFT curves, a full holistic picture of slagging and fouling can be produced for a fuel. The FactSage data showed an excellent relationship to the OAAFT curve. Herein, both experiment and FactSage modelling have verified the different strengths of CaO, Fe_2O_3, and MgO on the ash network and in particular the synergetic effects that could come into play for additive mixtures in practical utilisations. By combining OAAFT and FactSage data, power generators can replicate slagging and fouling issues and identify the major components which are causing issues. Following this, mineral additives of varying quantities can be tested to analyse how slagging and fouling issues can be tackled for specific fuels. This will be of increasing importance as fuel blending and new complex fuels such as refuse derived fuels enter the market.

Declaration of competing interest

The authors declare that they have no known competing financial interests or personal relationships that could have appeared to influence the work reported in this paper.

Acknowledgements

This work was supported by the Engineering and Physical Sciences Research Council (EPSRC), Centre of Doctoral Training in Carbon Capture and Storage and Cleaner Fossil Energy [grant number EP/L016362/1] and the International Young Scientist Research Fellowship, the Natural Science Foundation China (NSFC) [grant number 51650110508], and the University of Nottingham Anne McLaren Research Fellowship. A

special thanks to Carbolite-Gero for supplying the CAF furnace and the continual support throughout the research. The authors would like to thank all those involved in the project for their support and assistance.

References

[1] H. Shi, Y. Wu, M. Zhang, Y. Zhang, J. Lyu, Ash deposition of Zhundong coal in a 350 MW pulverized coal furnace: influence of sulfation, Fuel (2020) 260.
[2] C. Zhu, H. Tu, Y. Bai, D. Ma, Y. Zhao, Evaluation of slagging and fouling characteristics during Zhundong coal co-firing with a Si/Al dominated low rank coal, Fuel 254 (2019), 115730.
[3] R.W. Bryers, Fireside slagging, fouling, and high-temperature corrosion of heat-transfer surface due to impurities in steam-raising fuels, Prog Energy Combust Sci 72 (1995).
[4] P.P. Płaza, The Development of a Slagging and Fouling Predictive Methodology for Large Scale Pulverised Boilers Fired with Coal/Biomass Blends, University of Cardiff, 2013.
[5] T.F. Wall, R.a. Creelman, R.P. Gupta, S.K. Gupta, C. Coin, A. Lowe, Coal ash fusion temperatures—new characterization techniques, and implications for slagging and fouling, Prog Energy Combust Sci 24 (1998) 345–353.
[6] S. Gupta, T.F. Wall, R.A. Creelman, R. Gupta, Ash fusion temperatures and the transformations of coal ash particles to slag, Fuel Process Technol 56 (1998) 33–43.
[7] H. Kahraman, A.P. Reifenstein, C.D.A. Coin, Correlation of ash behaviour in power stations using the improved ash fusion test, Fuel 78 (1999) 1463–1471.
[8] S.V. Loo, J. Koppejam, Handbook of Biomass Combustion and Co-firing, 2008.
[9] I.W. Cumming, W.I. Joyce, J.H. Kyle, Advanced techniques for the assessment of slagging and fouling propensity in pulverized coal fired boiler plant, J Inst Energy (1985) 169–175.
[10] D.H.H. Quon, S.S.B. Wang, T.T. Chen, Viscosity Measurements of Slags from Western Canadian Coals, 1984.
[11] S.A. Lolja, H. Haxhi, R. Dhimitri, S. Drushku, A. Malja, Correlation between ash fusion temperatures and chemical composition in Albanian coal ashes, Fuel 81 (2002) 2257–2261.
[12] G. Dunnu, J. Maier, G. Scheffknecht, Ash fusibility and compositional data of solid recovered fuels, Fuel 89 (2010) 1534–1540.
[13] J.W. Regan, Impact of coal characteristics on boiler design, Coal Technol 3 (1982).
[14] J.C. Van Dyk, L.L. Baxter, J.H.P. Van Heerden, R.L.J. Coetzer, Chemical fractionation tests on South African coal sources to obtain species-specific information on ash fusion temperatures (AFT), Fuel 84 (2005) 1768–1777.
[15] M. Seggiani, Empirical correlations of the ash fusion temperatures and temperature of critical viscosity for coal and biomass ashes, Fuel 78 (1999) 1121–1125.
[16] J.C. Van Dyk, S.A. Benson, M.L. Laumb, B. Waanders, Coal and coal ash characteristics to understand mineral transformations and slag formation, Fuel 88 (2009) 1057–1063.
[17] T.F. Wall, S.K. Gupta, R.P. Gupta, R.H. Sanders, R.A. Creelman, G.W. Bryant, False deformation temperatures for ash fusibility associated with the conditions for ash preparation, Fuel 78 (1999) 1057–1063.
[18] A.C. Fieldner, A.E. Hall, A.L. Feild, The fusibility of coal ash and the determination of the softening temperature, Bur Mines 129 (1918) 19.
[19] C.H. Pang, B. Hewakandamby, T. Wu, E. Lester, An automated ash fusion test for characterisation of the behaviour of ashes from biomass and coal at elevated temperatures, Fuel 103 (2013) 454–466.
[20] P.J. Daley, O. Williams, C. Heng Pang, T. Wu, E. Lester, C.H. Pang, et al., The impact of ash pellet characteristics and pellet processing parameters on ash fusion behaviour, Fuel 251 (2019) 779–788, https://doi.org/10.1016/j.fuel.2019.03.142.
[21] E. Jak, S. Degterov, P.C. Hayes, A.D. Pelton, Thermodynamic modelling of the system Al2O3-SiO2-CaO-FeO-Fe2O3 to predict the flux requirements for coal ash slags, Fuel 77 (1998) 77–84.
[22] X. Li, L. Zhi, W. Shi, L. Kong, J. Bai, J. Yu, et al., Effect of K2O/Na2O on fusion behavior of coal ash with high silicon and aluminum level, Fuel 265 (2020), 116964, https://doi.org/10.1016/j.fuel.2019.116964.
[23] W.J. Shi, L.X. Kong, J. Bai, J. Xu, W.C.W. Li, Z.Q. Bai, et al., Effect of CaO/Fe2O3 on fusion behaviors of coal ash at high temperatures, Fuel Process Technol 181 (2018) 18–24, https://doi.org/10.1016/j.fuproc.2018.09.007.
[24] Y. Niu, H. Tan, X. Wang, Z. Liu, H. Liu, Y. Liu, et al., Study on fusion characteristics of biomass ash, Bioresour Technol 101 (2010) 9373–9381.
[25] Q.H. Li, Y.G. Zhang, A.H. Meng, L. Li, G.X. Li, Study on ash fusion temperature using original and simulated biomass ashes, Fuel Process Technol 107 (2013) 107–112.
[26] W.J. Song, L.H. Tang, X.D. Zhu, Y.Q. Wu, Z.B. Zhu, S. Koyama, Effect of coal ash composition on ash fusion temperatures, Energy and Fuels 24 (2010) 182–189.
[27] B. Liu, Q. He, Z. Jiang, R. Xu, B. Hu, Relationship between coal ash composition and ash fusion temperatures, Fuel 105 (2013) 293–300.
[28] T. Yan, J. Bai, L. Kong, Z. Bai, W. Li, J. Xu, Effect of SiO2/Al2O3on fusion behavior of coal ash at high temperature, Fuel 193 (2017) 275–283.
[29] E. Jak, Prediction of coal ash fusion temperatures with the F*A*C*T thermodynamic computer package, Fuel 81 (2002) 1655–1668.
[30] M. Reinmöller, M. Sieradzka, M. Laabs, M. Schreiner, A. Mlonka-Mędrala, A. Kopia, et al., Investigation of the thermal behaviour of different biomasses and properties of their low- and high-temperature ashes, Fuel (2021) 301.
[31] H. Beidaghy Dizaji, T. Zeng, H. Hölzig, J. Bauer, G. Klöß, D. Enke, Ash transformation mechanism during combustion of rice husk and rice straw, Fuel 307 (2022).
[32] H. Yang, J. Jin, D. Liu, F. Hou, Y. Hang, The effect on ash deposition by blending high-calcium Zhundong coal with vermiculite: focusing on minerals transformations, Asia-Pacific J Chem Eng 16 (2021) 1–13.
[33] G. Yang, Q. Ren, J. Xu, Q. Lyu, Co-melting properties and mineral transformation behavior of mixtures by MSWI fly ash and coal ash, J Energy Inst 96 (2021) 148–157.
[34] F. Li, B. Yu, G. Wang, H. Fan, T. Wang, M. Guo, et al., Investigation on improve ash fusion temperature (AFT) of low-AFT coal by biomass addition, Fuel Process Technol 191 (2019) 11–19.
[35] L.S. Mokhahlane, M. Gomo, D. Vermeulen, Temperature and electrical conductivity stratification in the underground coal gasification zone and surrounding aquifers at the Majuba pilot plant, J South African Inst Min Metall 118 (2018) 1053–1058.
[36] W.J. Song, L.H. Tang, X.D. Zhu, Y.Q. Wu, Z.B. Zhu, S. Koyama, Prediction of Chinese coal ash fusion temperatures in Ar and H2 atmospheres, Energy and Fuels 23 (2009) 1990–1997.
[37] M. Reinmöller, L. Kong, M. Laabs, Z. Ge, C. Hommel, M.M. Farid, et al., Methods for the determination of composition, mineral phases, and process-relevant behavior of ashes and its modeling: a case study for an alkali-rich ash, J Energy Inst 100 (2022) 137–147.
[38] B.S. Methods, For Analysis and Testing of Coal and Coke. Analysis of Coal Ash and Coke Ash, 2017.
[39] J.A. Canny, Computational approach to edge detection, IEEE Trans Pattern Anal Mach Intell 8 (1986) 679–698. PAMI.
[40] N. Otsu, A threshold selection method from grey-level histograms, IEEE Trans Syst Man Cybern 9 (1979) 62–66.
[41] A. Seif, M.M. Salut, M.N. Marsono, A hardware architecture of Prewitt edge detection, IEEE conference on sustainable utilization and development in engineering and technology (2010) 99–101 (IEEE Confe), In press, https://ieeexplore.ieee.org/abstract/document/5686999/.
[42] D. Bradley, G. Roth, Adaptive thresholding using the integral image, J Graph Tools 12 (2007) 13–21.
[43] M. Reinmöller, M. Schreiner, S. Guhl, M. Neuroth, B. Meyer, Ash behavior of various fuels: the role of the intrinsic distribution of ash species, Fuel 253 (2019) 930–940.
[44] S. Vargas, F.J. Frandsen, K. Dam-Johansen, Rheological properties of high-temperature melts of coal ashes and other silicates, Prog Energy Combust Sci 27 (2001) 237–429.
[45] B.C. Pearce, J.W.F. Hill, I. Kerry, Use of x-ray fluorescence spectrometry for the direct multi-element analysis of coal powders, Analyst 115 (1990) 1397–1403.
[46] M. Reinmöller, M. Klinger, M. Schreiner, H. Gutte, Relationship between ash fusion temperatures of ashes from hard coal, brown coal, and biomass and mineral phases under different atmospheres: a combined FactSage™ computational and network theoretical approach, Fuel 151 (2015) 118–123.
[47] S.V. Vassilev, D. Baxter, C.G. Vassileva, An overview of the behaviour of biomass during combustion: Part I. Phase-mineral transformations of organic and inorganic matter, Fuel 112 (2013) 391–449.
[48] M. Reinmöller, M. Schreiner, S. Guhl, M. Neuroth, B. Meyer, Formation and transformation of mineral phases in various fuels studied by different ashing methods, Fuel 202 (2017) 641–649.
[49] J. Lachman, M. Baláš, M. Lisý, H. Lisá, P. Milčák, P. Elbl, An overview of slagging and fouling indicators and their applicability to biomass fuels, Fuel Process Technol (2021) 217.
[50] H. Namkung, L.H. Xu, T.J. Kang, D.S. Kim, H.B. Kwon, H.T. Kim, Prediction of coal fouling using an alternative index under the gasification condition, Appl Energy 102 (2013) 1246–1255.
[51] C.W. Bale, E. Bélisle, P. Chartrand, S.A. Decterov, G. Eriksson, A.E. Gheribi, et al., Reprint of: FactSage thermochemical software and databases, 2010–2016, Calphad Comput Coupling Phase Diagrams Thermochem 55 (2016) 1–19.
[52] J.C. Van Dyk, M.J. Keyser, Influence of discard mineral matter on slag-liquid formation and ash melting properties of coal - a FACTSAGE™ simulation study, Fuel 116 (2014) 834–840.
[53] T. Yan, L. Kong, J. Bai, Z. Bai, W. Li, Thermomechanical analysis of coal ash fusion behavior, Chem Eng Sci 147 (2016) 74–82.
[54] X.D. Chen, L.X. Kong, J. Bai, Z.Q. Bai, W. Li, Study on fusibility of coal ash rich in sodium and sulfur by synthetic ash under different atmospheres, Fuel 202 (2017) 175–183.
[55] D. Schwitalla, M. Reinmöller, C. Forman, C. Wolfersdorf, M. Gootz, J. Bai, et al., Ash and slag properties for co-gasification of sewage sludge and coal: an experimentally validated modeling approach, Fuel Process Technol 175 (2018) 1–9.
[56] D. Manara, R. Böhler, L. Capriotti, A. Quaini, Z. Bao, K. Boboridis, et al., On the melting behaviour of calcium monoxide under different atmospheres: a laser heating study, J Eur Ceram Soc 34 (2014) 1623–1636.
[57] European Chemicals Agency (ECHA), Calcium carbonate, SCIP Database, 2022 text=The melting point of calcium,decomposes into CaO and CO2, https://echa.europa.eu/registration-dossier/-/registered-dossier/16050/4/3#. (Accessed 11 April 2022).
[58] A. Luxsanayotin, S. Pipatmanomai, S. Bhattacharya, Effect of mineral oxides on slag formation tendency of mae moh lignites, Songklanakarin J Sci Technol 32 (2010) 403–412.
[59] T. Kupka, M. Mancini, M. Irmer, R. Weber, Investigation of ash deposit formation during co-firing of coal with sewage sludge, saw-dust and refuse derived fuel, Fuel 87 (2008) 2824–2837.
[60] M. Seggiani, G. Pannocchia, Prediction of coal ash thermal properties using partial least-squares regression, Ind Eng Chem Res 42 (2003) 4919–4926.

[61] G. Zhang, M. Reinmöller, M. Klinger, B. Meyer, Ash melting behavior and slag infiltration into alumina refractory simulating co-gasification of coal and biomass, Fuel 139 (2015) 457–465.
[62] S.V. Vassilev, D. Baxter, L.K. Andersen, C.G. Vassileva, An overview of the chemical composition of biomass, Fuel 89 (2010) 913–933.
[63] L. Yan, R.P. Gupta, T.F. Wall, The implication of mineral coalescence behaviour on ash formation and ash deposition during pulverised coal combustion, Fuel 80 (2001) 1333–1340.
[64] W. Xuan, J. Zhang, D. Xia, The influence of MgO on the crystallization characteristics of synthetic coal slags, Fuel 222 (2018) 523–528, https://doi.org/10.1016/j.fuel.2018.02.197.
[65] L. Zhang, J. Wang, J. Wei, Y. Bai, X. Song, G. Xu, et al., Synergistic effects of CaO and MgO on ash fusion characteristics in entrained-flow gasifier, Energy and Fuels 35 (2021) 425–432, https://doi.org/10.1021/acs.energyfuels.0c03358.
[66] G.W. Bryant, G.J. Browning, H. Emanuel, S.K. Gupta, R.P. Gupta, J.A. Lucas, et al., The fusibility of coal ash, Energy Fuel (2000) 316–325.
[67] L. Guo, M. Zhai, Z. Wang, Y. Zhang, P. Dong, Comprehensive coal quality index for evaluation of coal agglomeration characteristics, Fuel 231 (2018) 379–386, https://doi.org/10.1016/j.fuel.2018.05.119.
[68] X. Shi, Y. Zhang, X. Chen, Y. Zhang, Effects of thermal boundary conditions on spontaneous combustion of coal under temperature-programmed conditions, Fuel 295 (2021), 120591.
[69] J.H. Kim, G.B. Kim, C.H. Jeon, Prediction of correlation between ash fusion temperature of ASTM and Thermo-Mechanical Analysis, Appl Therm Eng 125 (2017) 1291–1299.
[70] M.B. Folgueras, R.M. Díaz, J. Xiberta, M.P. García, J.J. Pis, Influence of sewage sludge addition on Huainan coal ash fusion characteristics, Energy & Fuels 19 (2005) 2562–2570.
[71] W. Shi, M. Laabs, M. Reinmöller, J. Bai, S. Guhl, L. Kong, et al., In-situ analysis of the effect of CaO/Fe2O3 addition on ash melting and sintering behavior for slagging-type applications, Fuel 285 (2021), 119090.
[72] A. Mlonka-Mędrala, T. Dziok, A. Magdziarz, W. Nowak, Composition and properties of fly ash collected from a multifuel fluidized bed boiler co-firing refuse derived fuel (RDF) and hard coal, Energy (2021) 234, https://doi.org/10.1016/j.energy.2021.121229.